Chapter 9
Molecular-Plasmon Nanostructures for Biomedical Application

Alexey Povolotskiy, Marina Evdokimova, Alexander Konev, Ilya Kolesnikov, Anastasia Povolotckaia and Alexey Kalinichev

Abstract The development of modern nanotechnology opens new opportunities in the design of hybrid structures. This review is devoted to the general view on hybrids, which are based on metal nanoparticles and molecules. Functional properties of nanostructures that have a biomedical application are presented, including singlet oxygen generation for photodynamic therapy, photo-induced heating for photothermal therapy, photo-induced reactions for chemotherapy, luminescent thermometry and surface enhanced Raman scattering for drug delivery control etc. The association of nanostructures into hybrids allows to combine their functional properties and create universal preparations for controlled complex therapy.

9.1 Introduction

Over the years, the development of new cancer treatment strategies has been a priority for health care system. There are a number of issues and problems of oncology, the solution of which will significantly improve therapy methods. The central concern of scientists is to overcome multiple drug resistance, reduce anti-cancer drugs toxicity, and develop non-invasive methods. In order to demonstrate the effectiveness of the abovementioned strategy, materials should have specific physicochemical properties and ability to integrate different anti-cancer modalities, such as chemotherapy, photothermal therapy (PTT) and photodynamic therapy (PDT) into a single nanoplatform [1, 2]. Currently, latest publications and studies have demonstrated successful synthesis and in vivo experiments of these multifunctional systems based on hybrid metallic nanostructures in biomedical applications [3–7]. To create hybrid nanostructures, noble nanoparticles are usually used as nanocarrier forming the basis of surface coatings for various functionalities [8–10]. Different components have been used to modify nanomaterial surfaces for reaching desired properties and applications: small molecule drugs, biologic medical products, luminescent and photosensitive components. According to this approach, such class of nanohybrids is attracting

A. Povolotskiy (✉) · M. Evdokimova · A. Konev · I. Kolesnikov · A. Povolotckaia · A. Kalinichev
Saint-Petersburg State University, Saint-Petersburg, Russia
e-mail: alexey.povolotskiy@spbu.ru

K. Yamanouchi et al. (eds.), *Progress in Photon Science*, Springer Series in Chemical Physics 119, https://doi.org/10.1007/978-3-030-05974-3_9

considerable attention because of the possibility for controlling the incorporation of light-activated nanoparticles into tumors, minimizing the damage in the surrounding healthy tissue, combining both diagnostic and therapeutic capabilities in one structure, known as theranostics approach [11].

9.2 Photothermal Therapy

Photothermal therapy (PTT) is a growing therapeutic method which leads to cell death in malignant tumor by an increase in temperature caused by hybrid metallic nanostructures upon NIR laser irradiation. The fast thermalization of gold nanoparticles (AuNPs) when selective absorption of light occurs, combined with the NIR plasmon resonance makes them ideal candidate as contrast agents for photothermal therapy (Fig. 9.1) [12, 13].

At present, four major types of AuNPs demonstrate efficient NIR photothermal heat conversion, including gold nanospheres [14, 15], nanorods [16, 17], nanoshells [18, 19], and nanocages [20, 21]. When the works deal with in vitro photothermal experiments, the effective destruction of the diseased tissue can be achieved by changing treatment conditions such as the power density, laser exposure duration, and the response time after irradiation. For photothermal treatment, typical intensities are considered to range from 1 to 100 W/cm^2 using continuous wave laser [22]. Kang's group synthesized novel GNRs-porphyrin-trastuzumab complexes (TGNs) using gold nanorods (GNRs) conjugated with porphyrin and trastuzumab (anti-HER2 antibody) to target to HER2-positive breast cancer for NIR light-activatable photothermal therapy [16]. The nanohybrids had an excellent photothermal effect in vitro under 808 nm (with an intensity of 6.07 W/cm^2) laser exposure for 12 min. A significant photothermal effect had induced tumor reduction, which was reached after TGNs-injection into tumor-bearing mice models. Compared with alone GNRs or porphyrin, the hybrid TGNs with lower cytotoxicity showed durable elevated temperature to around 56 °C, high enough to cause tumor ablation. As expected, the

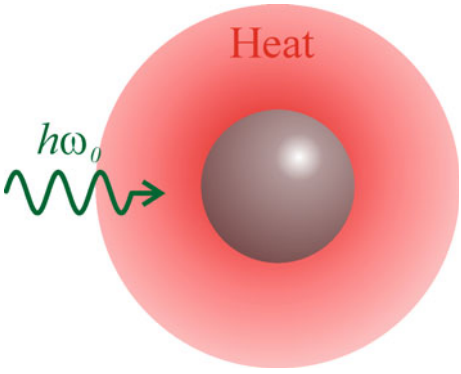

Fig. 9.1 Photo-induced thermalization of gold nanoparticles

in vivo experiments showed different effects for the following control groups such as TGNs nanohybrids only, TGNs + laser, and GNR + laser. The breast cancer-bearing nude mice in TGNs + laser group were nearly healed at 12 days. Moreover, the pathological changes in tumors indicated the significantly higher apoptosis index of cancer cells when compared with the control group. Therefore, the TGNs nanohybrids represented a great agent for photothermal treatment of tumor in vivo.

In addition, gold nanoparticles coated over a silver core exhibited even better photothermal conversion properties than the free gold nanoparticles. Shi et al. [23] synthesized Au@Ag/Au nanoplatform assembled with activatable probes containing thiolated aptamer and fluorophore-labeled complementary DNA for image-guided cancer therapy in vitro and in vivo. In these nanohybrids, Au@Ag/Au nanoparticles manifested dual functionality as both fluorescence quenchers and optical heaters. They obtained excellent results in selective activation of fluorescence signal during conformational reorganization of aptamer and targeting activatable theranostic nanoprobe to A549 lung cancer cells. Recently, in addition to selective destroy of targeted cancer cells through photothermal therapy, other mechanisms of AgNP-induced cancer cell death have extensively been proposed, such as endoplasmic reticulum stress (ER), reactive oxygen species (ROS), upregulation of autophagy genes [24–26]. Platinum-based nanomaterials could also be applied for PTT. For example, Chen's group realized green one-step synthesis of biocompatible fluorescent platinum nanoclusters (Pt NCs) by reducing chloroplatinic acid with ascorbic and glutathione acid for the bio-imaging and photothermal treatment of target cancers [27]. In other work, Chen et al. established a new effect of spontaneous synthesis of platinum nanoclusters by cancer cells and tissues via their propensity to generate both H_2O_2 and ROS through dioxygen reductions. Also, they improved image-guided PTT by combining porphyrin derivative 5,10,15,20-tetrakis(4-sulfonatophenyl)porphyrin (TSPP) with Pt NCs [28]. However, in most cases, systemic toxicity and large size of platinum nanoparticles doesn't allow them to be used for anti-cancer therapy [29].

9.3 Photodynamic Therapy

The integration of photoactive molecules (photosensitizers) in hybrid metallic nanostructures allow to significantly improve therapeutic efficacy of nanoparticles and apply them not only in photothermal (PTT), but also in photodynamic therapy (PDT). Therefore, photosensitizer-coated nanoparticles (NPs) have been reported to achieve highly promising results for PDT in several animal models [30]. This approach requires selective absorption of the photosensitizers (PSs) by the cancer cell and its further laser irradiation. As a result, photoactive molecule goes into excited triplet state, transfers accumulated energy to the surrounding oxygen molecules for producing reactive oxygen species (ROS) such as singlet oxygen ($^1O_2$) (Fig. 9.2) or free radicals, thus killing cancer cells [31].

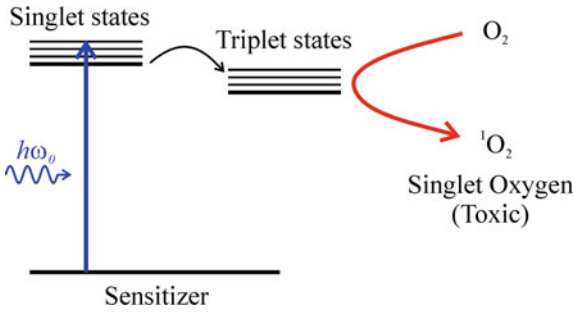

Fig. 9.2 Photo-induced generation of singlet oxygen

Moreover, introduction of some heavy atoms (e.g. Br and I) on a PS has been reported to increase intersystem crossing rates, leading to higher ROS generation [32, 33]. It should be noted that many examples combine NPs and photosensitizers, especially porphyrins and phtalocyanines. Several groups [34–36] demonstrated both PDT efficacy of porphyrin-functionalized GNPs and significant influence on the viability of different class of cancer cell line in vitro and in vivo in comparison with the free ligands. In these published works, protoporphyrin, hematoporphyrin, and brucine–porphyrin derivatives were used to functionalize GNPs. Dissymmetrical porphyrin derivatives having one alkyl chain with a thiol end group incorporating to phenyl group is proposed in the search for new photosensitizers. Penon's group synthesized novel water-soluble multifunctional nanosystem with low intrinsic toxicity comprising of gold nanoparticles (GNP-PR/PEG) immobilized 5-[4(11-mercaptoundecyloxy)-phenyl-10,15,20-triphenylporphyrin (PR-SH) and thiolated polyethylene glycol, which were used as advanced nanotheranostic agents for PDT [37]. Thus, they proved the capability to incorporate a lipophilic PS onto the GNP surface that increases the water solubility of the nanosystem. To evaluate the photodynamic activity nanohybrids, various chemical quenchers are used to characterize the amount of ROS after laser irradiation by monitoring fluorescence intensity of dyes [38, 39].

For enhancing the photodynamic therapy (PDT) efficacy in the near infrared (NIR) range against human breast cancer cells (MDA-MB-231), Hua and co-workers reported a layer-by-layer (LbL) assembly method to realize precise microfabrication of nanostructures consisted of gold nanorings (AuNRs) coated with two layers of Al(III) phthalocyanine chloride tetrasulfonic acid ($AlPcS_4$) [40]. It is revealed that deposition of two $AlPcS_4$ layers had increased the PDT of cancer cells in the NIR by a factor of 8 (is about ~85% cancer cells) compared with $AlPcS_4$ only or the Au NR-$AlPcS_4$ mixture. In absence of NIR radiation, the porphyrin photosensitivity adsorbed on the Au NR surface is inhibited due to charge-transfer induced quenching. During NIR irradiation, the dye is highly activated upon release of the PS from and in the immediate vicinity of the Au NRs resulting in field-enhanced ROS generation. Thus, this strategy, recommended by other researchers, has been successfully employed for constructing interesting nanostructured assemblies that display a high ROS yield [41, 42].

9.4 Combined Photothermal and Photodynamic Therapies

The integrated PTT and PDT nanoplatform is designed to achieve moderate hyperthermia (<45 °C) for less invasive cancer cell death and reactive oxygen species (ROS)-mediated intracellular damage, thus obtaining improved anti-cancer efficacy [43]. The treatment efficiency and the synergistic effect of PDT and PTT can be reached, if the photosenstisizer and photothermal agent are simultaneously delivered to cancer cells in a specific location. Thus, recent investigations are primarily focused on the PS-photothermal agent hybrid nanostructures for collaborative PDT/PTT therapy triggered by a single NIR laser [43, 44]. Using abovementioned strategy, Kumar et al. developed hybrid core-petal nanostructures (CPNs) for PDT–PTT-based apoptotic therapeutics realized through the gold chloride-induced oxidative disassembly and rupture of the polydopamine corona around Au nanoparticles and subsequent anisotropic growth of Au nanopetals with various protrusion lengths and densities. It was reached the efficient killing of cancer cell with CPN-4 (with maximum density of nanopetals) at mild increase in temperature (~42 °C) under 785 nm laser power density of 2 W/cm^2 for 6 min [45]. Photosensitizer-conjugated gold nanostars have been prepared by Wang's group, showing combined PDT and PTT effects using single wavelength NIR laser and improved cancer therapy efficacy in MDA-MB-435 tumour-bearing mice [44]. Nevertheless, the simultaneous synergistic therapy directly depends on the overlap both optical absorption of photosenstisizer and photothermal agent. Unfortunately, there are almost no articles conceptualizing the PDT/PTT combination treatment because of the particular requirement and complicated synthesis [46, 47].

Many NIR dyes from porphyrin family are clinically approved by the U.S. Food and Drug Administration (FDA). Their molecules can convert the absorbed light energy to local hyperthermia for PDT and PTT and ROS generation. Therefore, porphyrin derivatives could be considered as a kind of ideal theranostic platform for biomedical applications. Recently, several research groups have applied gold nanoparticles as nanocarriers to prepare porphyrin-coated NPs for improving stability and tumour-specificity.

For example, gold-nanoclustered hyaluronan nanoassembly (GNc-HyNA) has been developed as a nanomedicine platform. For the synthesis of the hybrid nanomaterials were employed amphiphilic hyaluronan-polycaprolactone (Hy-PCL) conjugates as a drug carrier for a hydrophobic photodynamic therapy agent verteporfin (V_p), a polymeric reducing agent and an organic nanoscaffold, into a single nanoplatform [48]. Both in vitro and in vivo experiments demonstrated that GNc-HyNA loaded verteporfin exhibited excellent stability in the bloodstream and exerted a great potential to treat tumors with a 100% survival rate. Thus, it is proved that V_p-GNc-HyNA can potentially be applied for photothermally boosted photodynamic tumor ablation.

In addition, Zeng's and Lokesh's group reported that Au NPs coated with cobalt and manganese porphyrin derivatives can be used for the development of the artificial photosynthetic and catalytic materials [49, 50]. Recently, it has been reported that

combination of meso-tetrakis(4-sulphonatophenyl)porphyrin (TPPS) and chitosan-coated Au NPs (TPPS/QCS-SH/Au NPs) contributed to development novel nanoplatform system with improved photoproperties, including excellent biocompatibility, stability, high $^1O_2$ generation and photothermal conversion efficiency, due to synergistic effect of PDT and PTT [51]. Lin's group synthesized Chlorin e6 (C6)-encapsulatedplasmonic gold vesicles (GV-Ce6) for dual-modality PTT/PDT cancer treatment. The tumor treatment efficiency of the GV-Ce6 nanohybrids were demonstrated be higher than the sum effect of individual GVs and Ce6 components, representing a more effective tumor localized therapy [52].

9.5 Combined Chemo-photothermal Therapy

In contrast to traditional chemotherapy, in which drugs spread freely in the bloodstream resulting in the cytotoxicity both cancer and healthy cells [53, 54], a new approach enable the optically controlled delivery of drugs based on photothermal reaction mechanism. It means that drug delivery could be achieved through the light-heat activation of nanoparticles after they absorb light. The activation causes the local temperature increase and the release of drugs from the drug carrier along with photothermal ablation treatment due to thermal energy production. This approach can not only potentially increase drug bioavailability and capacity to overcome physical barriers, but also reduce the dosage to be used for treatment, thus reducing the toxic side effects [55].

Several nanocarrier options have been pursued, depending on the type of tumor cells and desired functions [10, 56, 57]. Khandelia's group studied the possibility to use AuNS–protein agglomerate-based nanohybrids as multimodal drug-delivery vehicles against cancer cells. Albumin stabilized agglomerated structures of gold nanoparticle (Au NP)–lysozyme (Lyz) have been fabricated, showing high drug-loading and-releasing capabilities for both hydrophilic doxorubicin (DOX) and hydrophobic pyrene (PYR) molecules [10]. DOX release was done via changes in pH value of the media inside the cell and was 35% at pH 4.0 and 27% at pH 7.4 up to 24 h, while any release of PYR wasn't observed in both the buffers due to strong binding of PYR in the hydrophobic regions of agglomerates. In another study, Lee and co-workers proposed AuNPs as carriers in target-specific systemic treatment of hepatitis C virus (HCV) infection [58]. New developed HA-AuNPs/IFNα complex for targeted systemic treatment based on interferon α (IFNα) loaded on thiolated HA-modified AuNPs (HA-AuNPs) have demonstrated an enhanced serum stability in human serum and prolonged efficacy in liver tissue for the treatment of chronic HCV infection.

DOX is one of the most widely used anti-cancer agents, causing inhibition of the progression of the enzyme topoisomerase II which leads to inhibition of cell growth and reproduction by interferencing DNA replication. The mechanism of drug release to cause DNA damage is the key of combined chemo-photothermal therapy. Chen et al. developed the tumor-targeting nanoplatform AuNS-pep/DOX@HA by

using gold nanostar (AuNS) bearing peptide TPP-KLA and DOX encapsulated in hyaluronic acid (HA) protective shell [56]. It was proved that nanoplatform selectively accumulates at tumor site and the internalization mechanism into tumor cells occurs via CD44 receptor-mediated recognition. Followed degradation of HA by hyaluronidase (HAase), the therapeutic AuNS-pep/DOX@HA system demonstrated the ability to release DOX for chemotherapy and mitochondria-targeting/anchoring heat generator AuNS-pep for NIR light triggered subcellular photothermal therapy (PTT). Both in vitro and in vivo experiments showed that the AuNS-pep/DOX@HA nanoplatform has an ability to be a prominent non-resistant or resistant tumor inhibition. New nanotheranostic agent of DOX@PLA@Au-PEG-MnP has been developed by Jing et al. [7] integrating different functionalities in single nanoplatform. Hybrid drug delivery system made of various components, including: (1) poly(lactic acid) (PLA) as biodegradable drug carrier; (2) gold nanoshell as NIR photo-absorber to perform photothermal therapy and trigger an instant drug release; (3) Mn-porphyrin (MnP) as T_1 contrast agent to enhance MR imaging, and PEG to extend the circulation time in vivo experiments. This multifunctional nanoparticle manifested its photothermal therapeutic potential and triggered DOX release activated during NIR irradiation of Au nanoshells on both cellular experiments and HT-29 tumor-bearing nude mice. Systemic toxicity studies conducted in mice revealed that hybrid DOX@PLA@Au-PEG-MnP nanoparticle combined DOX and photothermal treatment were more cytotoxic than either agent alone in the treatment. Wang's group used the same chemotherapeutic agent in multi-stimuli responsive nanoplatform for targeted, non-invasive and pinpointed intracellular DOX release, which consisted of Au nanocages, hyaluronic acid (HA) and DOX encapsulated in gold nanocages@hyaluronic acid (AuNCs-HA) [59]. In vitro results confirmed efficiently drug-loaded nanohybrids uptake by cancer cells via interactions of hyaluronic acid with CD44 active sites holding significant importance in modulating targeting ability of hyaluronic acid to different cancer types and subsequently intracellular degradation into small fragments, releasing DOX. On the other hand, in vivo experiments have further revealed that AuNCs-HA nanohybrids demonstrate biocompatibility, CD44-targetability, multi-stimuli responsiveness, pinpointed drug release and chemo-photothermal synergistic effects and thus, have a great potential application in cancer therapy.

9.6 Triple Combination Nanotherapeutics

Although combined therapy of PTT/PDT, PDT/chemotherapy, and PTT/chemotherapy has been reported to enhance therapeutic efficiencies, it remains in the early stages and certain limitations still exist, including of the residual cancer cells survival after photothermal damage, the PDT-induced hypoxia microenvironment and hypermethylated cancer cell resistance to chemotherapeutic drugs [60, 61]. Therefore, an alternative approach was created for further improving therapeutic efficacy. Zeng's group used core–shell gold nanorod@metal–organic frameworks (AuNR@MOFs) made up of gold nanorods functionalized with

lipoic acid and poly(ethylene glycol) (PEG)-SH polymer to develop organic nanotheranostic agents with triple-modal therapy. As a photodynamic agent was used tetrakis (4-carboxyphenyl)porphyrin) consisting of 6-connected Zr_6 cluster ($Zr_6O_4(OH)_4(H_2O)_6(OH)_6(COO)_6$) and tetratopic linker (TCPP) and drug (CPT: camptothecin) through π–π stacking and electrostatic interaction were loaded [6]. In this as-prepared nanoparticle, not only the loading of porphyrinic MOF on AuNR@(PEG)-SH could accelerate cellular uptake, but also the photothermal effect of porphyrinic MOF could promote drug delivery, enabling combined photodynamic, photothermal and chemotherapy for synergistic damaging the tumor cells in vitro and in vivo.

Park and co-workers prepared doxorubicin-loaded hollow gold nanoparticles (DOX-HGNPs) that demonstrated the effects of combined chemotherapy, thermal and radiotherapy [62]. The DOX release mechanism was triggered by an NIR laser and increased with irradiation. The triple-combination therapy strategy reduced tumor's weight by 6.8-fold and showed delayed tumor growth by 4.3-fold for A549 bearing mice compared to control groups. The radio-enhancing effect of DOX-HGNPs was confirmed by the high level of γ-H2AX (phosphorylated histone) foci than before the irradiation. CT imaging studies obtained were compared to the clinically available Ultravist 300 and HGNPs, showing a linear dependence of the absorption on the concentration and an attenuation coefficient higher than that of Ultravist 300.

9.7 Luminescent Probes and Sensors for Temperature

Temperature is one of the most fundamental parameter in all kinds of science. Respective sensors [63, 64] are widely used in daily life, in metrology, aerodynamics, climate and marine research, in chemistry, medicine, biology, military technology, air conditioning, in practically all devices for heating and cooling. The share of thermal sensors can be estimated as 75–80% of the world's sensor market [65]. Types of thermometers include liquid-filled glass thermometers based on the thermal expansion of materials [66]; thermocouples based on the Seebeck effect [67, 68]; and optical sensors [69]. All contact measurements require convective heat transfer and thus need to reach equilibrium between the sensor and the object. This procedure can alter the actual temperature of the object during the measurement, especially if the size of the sample is small. Moreover, traditional liquid-filled and bimetallic thermometers, thermocouples, pyrometers, and thermistors cannot be easily miniaturized and therefore are not suitable for temperature measurement with a spatial resolution of <10 μm which is desirable for micro/nanoelectronics, photonic devices and especially for various biological application.

Thermometry at the nanoscale requires, therefore, a new paradigm in the use of both materials and thermometric properties. Moreover, new synthetic techniques are helping to reduce materials limitation for sensing temperature at the nanoscale by either improving qualitatively inherent materials properties, e.g., size dispersion,

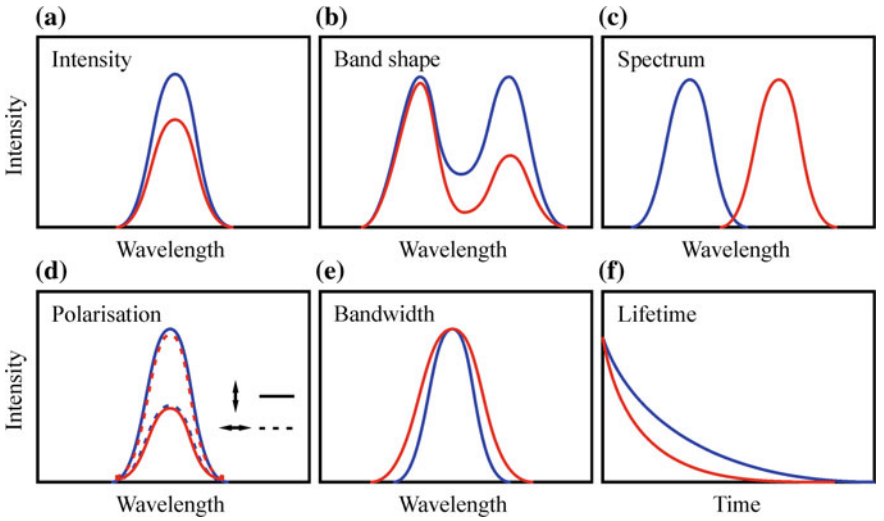

Fig. 9.3 Schematic representation of the possible effects caused by a temperature increment on the luminescence. Red lines correspond to higher temperatures

surface roughness, or by opening entirely new possibilities based on new materials with new properties. Recently luminescence thermometry becomes one of the most popular approaches to thermal sensing at nanoscale. This technique possesses unique properties including noninvasive, contactless, and simplicity of read-out [70]. Luminescence is the emission of light from a given substance, occurring from electronically excited states that have been populated by an external excitation source. The properties of the emitted photons depend on the characteristics of the electronic states involved in photon emission [71, 72]. These, in turn, depend on the local temperature and thus luminescence nanothermometry exploits the relationship between temperature and luminescence properties to achieve thermal sensing from the spatial and spectral analysis of the light generated from the object to be thermally imaged. Luminescence thermal sensors can be grouped into different classes based on the particular luminescent parameter which is analyzed and from which the thermal reading is ultimately extracted. Figure 9.3 schematically depicts the six parameters that characterize the emission of a given material: intensity, band-shape, spectral position, polarization, lifetime and bandwidth.

Figure 9.3 also qualitatively demonstrates how the luminescence emission spectrum is modified when each of these parameters is varied. Thus, based on these variations it is possible to define the following luminescence nanothermometry subclasses.

Intensity Luminescence Nanothermometry. In this case, thermal sensing is achieved through the analysis of the luminescence intensity. When temperature changes, there is an overall change in the number of emitted photons per second such that the emission spectrum becomes less (or more) intense. Temperature induced

changes in the luminescence intensity are generally caused by the thermal activation of luminescence quenching mechanisms and/or increases in the non-radiative decay probabilities.

One of the first examples reported the temperature dependence of the luminescent intensity of a naphthalene fragment covalently linked to a Ni(II) tetraazamacrocyclic complex, cyclam [73]. The intensity of the cyclam emission is partially quenched by an energy transfer mechanism whose efficiency decreases with temperatures between 300 and 338 K, resulting in a temperature dependent emission with a maximum relative sensitivity of 3.6% K^{-1} at 300 K. The luminescence intensity of Rhodamine B, which can be used as liquid solution or thin film, reduces linearly with temperature at a rate close to 2% per C, which is similar to that found for QDs [74–76]. Fluorescein covalently linked to starch responds linearly to temperature in the range from 273 to 333 K [77].

Band-Shape Luminescence Nanothermometry. The term "band-shape" refers to the relative intensity between the different spectral lines that make up the luminescence spectrum. Thermally induced variations in the band-shape usually take place when the electronic states from which emission is generated are very close in energy such that they are thermally coupled. It can be also present in mixed systems, i.e. systems containing more than one class of emitting centers. There are a great variety of examples in the literature that report on ratiometric luminescent systems including lanthanide complexes, quantum dots and organic dyes.

$[Tb_{0.99}Eu_{0.01}(hfa)_3(dpbp)]_n$ (hfa: hexafluoroacetylacetonato, dpbp: 4,4′-bis(diphenylphosphoryl) coordination polymer is a ratiometric probe (emission at 543 nm is sensitive to temperature, but the emission at 613 is not) with relative sensitivity of 0.83% K^{-1}, which can be utilized in temperature range of 200–500 K [78]. An example of a ratiometric highly sensitive molecular thermometer based on a platinum octaethyl porphyrin was described by Lupton [79]. The intensity ratio uses two transitions of the PtOEP (2,3,7,8,12,13,17,18-octaethyl-21H,23H-porphyrin platinum(II)): the first excited triplet level, at 650 nm, and one band, at 540 nm, which origin is not entirely clear. PtOEP is able to monitor temperature changes in the range 290–320 K with a maximum relative sensitivity of 4.6% K^{-1} at 305 K. A trizwitterionic dicationic Cu5 cluster exhibits an excellent thermochromic temperature-dependent luminescence in the range between 228 and 353 K with a high sensitivity and temporal (sub-millisecond) as well as spatial (sub-micrometer) resolution [80]. Chromium(III)-based dye was used an unprecedented molecular ratiometric thermometer in the 210–373 K temperature range in organic and in aqueous media [81].

Spectral Luminescence Nanothermometry. It is based on the analysis of the spectral positions of the emission lines, which are unequivocally determined by the energy separation between the two electronic levels involved in the emission. In turn, this depends on a large variety of temperature dependent parameters of the emitting material including refractive index and inter-atomic distances (density). Thus, in any emitting material the spectral positions of the luminescence lines are expected to

be temperature dependent, and this is exploited by spectral luminescence nanothermometry to translate spectral shifts into temperature. It should be noted that Spectral Luminescence Nanothermometry is not based on the analysis of absolute or relative intensities but on the determination of the spectral position of the luminescence lines. Consequently, temperature reading is not affected by luminescence intensity fluctuations caused by variations in the local concentration of emitting centers.

A pyrene-containing triarylboron molecule, DPTB (dipyren-1-yl(2,4,6-triisopropylphenyl)borane), dissolved in 2-methoxyethyl ether, shows temperature-dependent green to blue luminescence over the temperature range 223–373 K. The temperature can be determined by the blue-shift of the broad emission spectra, ascribed to the thermal equilibrium between twisted intramolecular charge transfer and local excited state of the DPTB molecule with 40 μm resolution [82]. Copper(I) cluster complexes give visually observable thermochromic shifts in luminescence [83–85]. Such probes cover a whole range from 8 to 290 K.

Polarization Luminescence Nanothermometry. In anisotropic media, the emitted radiation is generally non-isotropically polarized and consequently, the shape and intensity of emitted radiation are strongly dependent on its polarization. This allows the definition of the "polarization anisotropy" parameter, which is the ratio between the luminescence intensities emitted at two orthogonal polarization states. As a result, polarization luminescence nanothermometry is based on the influence of temperature on this polarization anisotropy.

One of the molecules used in the past for Polarization Luminescence Nanothermometry is fluorescein [86]. Its polarization anisotropy is modified by more than a 100% making it a highly sensitive temperature sensor. The green fluorescent protein (GFP) can also act as a thermal sensitive intracellular nanoprobe [87], because its fluorescence polarization anisotropy (FPA) depends on temperature. The method was applied to GFP-transfected HeLa and other cancer cell lines to monitor the heat generated after photothermal heating using gold nanorods surrounding the cells. A spatial resolution of 300 nm and a thermal resolution of about 0.4 K were achieved.

Bandwidth Luminescence Nanothermometry. The width of the various emission lines that make up any luminescence spectrum is determined by the properties of the material (such as the degree of disorder) and temperature. It is well-known that as the temperature of a luminescent material is increased, a corresponding increase in the density of phonons occurs resulting from the spectral contribution of homogeneous line broadening. Generally, in the vicinity of room temperature, homogeneous line broadening leads to a linear relationship between bandwidth and temperature. The change in the bandwidth of the luminescence spectra is exploited in bandwidth luminescence nanothermometry to achieve a thermal reading.

The magnitude of the temperature induced luminescence line broadening is in general small and thus, can be only observed in systems showing inherent narrow emission lines and in which homogeneous line broadening dominates over the inhomogeneous one. This is the case of rare earth ions incorporated in some crystalline hosts [88–91].

Lifetime Luminescence Nanothermometry. Luminescence lifetime is defined as the time that the emitted luminescence intensity decays down to 1/e of its initial value after a pulsed excitation. This is an indication of the total decay probability of the emitted intensity (indeed this probability is defined as the inverse of the luminescence lifetime). Decay probabilities from electronic levels depend on a great variety of factors and many of them are related to temperature (such as phonon assisted energy transfer processes and multiphonon decays). This temperature dependence makes it possible to extract temperature readings from the determination of the luminescence lifetime.

The temperature-induced reduction of the observed lifetime of luminescent organic dyes is a well-known phenomenon and is especially noticeable in the case of the Rhodamine B dye [92–94]. A luminescence lifetime reduction close to 75% is observed in the 10–70 °C range. The terbium(III) tris[(2-hydroxybenzoyl)-2-aminoethyl]amine chelate was found to be a viable probe for lifetime temperature sensing [95]. Molecular thermometer consists of [Eu(btfa)$_3$ (MeOH)(bpeta)] and [Tb(btfa)$_3$(MeOH)(bpeta)] β-diketonate chelates (btfa: 4,4,4-trifluoro-l-phenyl-1,3-butanedione, bpeta: bis(4–pyridyl)ethane) embedded into organic-inorganic hybrid nanoclusters formed by a maghemite (γ-Fe_2O_3) magnetic core coated with a tetraethyl orthosilicate/aminopropyltriethoxysilane organosilica shell demonstrated temperature dependence of luminescence lifetime in 14–300 K range [96]. A tetradecanuclear copper(I) cluster compound demonstrated temperature dependence of the emission decay lifetimes with Mott–Seitz model fitting [97].

Thus, we can conclude that luminescence nanothermometry provides several options to achieve thermal sensing from the analysis of the emission spectrum generated by the system under study.

One of the most promising thermal sensing techniques is based on Band-Shape Luminescence. Ratiometric temperature sensing can be achieved with three design concepts: (i) a combination of two emissive dyes (temperature-responsive probe and temperature-inert reference); (ii) a combination of two dyes which interact by a distance-dependent process, such as fluorescence resonance energy transfer (EnT) in systems, in which distance between dyes is modified by temperature; and (iii) a single dye displaying dual emission (Fig. 9.4) [72, 98–100].

First concept is commonly achieved by combining two phosphors in a fixed ratio (Fig. 9.4a). For example, both dyes must be excitable at the same wavelength and show spectrally distinguishable emission bands to allow separating and integrating the luminescence signals for the calculation of the temperature sensitive ratio I_{probe}/I_{ref}.

Fluorescent temperature sensors, which exploit temperature-dependent structural features connected with changes in fluorescence intensity of the reporter dyes are fluorophore-labeled molecular beacons (MBs) (Fig. 9.4b) [101–104]. These flexible single-stranded oligonucleotides are either dually labeled at their 5′- and 3′-ends with a fluorophore and a nonemissive quencher (nonratiometric MBs) or with two spectrally distinguishable emitters (ratiometric MBs). The fluorescence properties of these MBs are determined by the temperature-dependent conformation of the

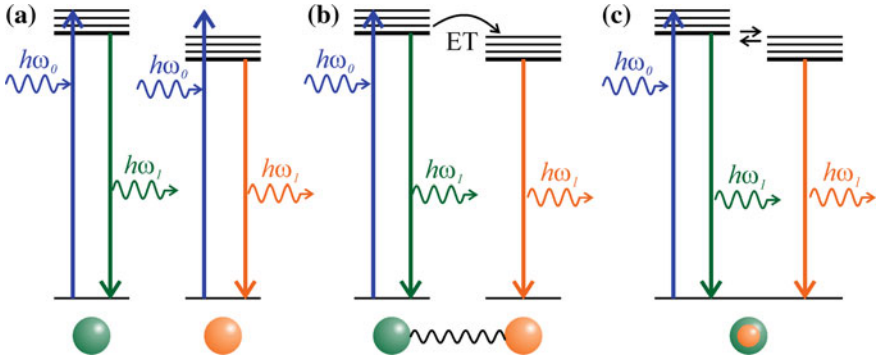

Fig. 9.4 Principles of dual-emission optical thermometers: **a** two distinct dyes; **b** two fluorophores interacting through energy transfer EnT; and **c** single dye with two equilibrating excited states

stem region, which defines the label distance. Because large molecular motions are involved, thermometers based on MBs are only operative in solution. The third scenario, internal referencing of the temperature-sensitive optical signal of a single dual emissive fluorophore, is principally more straightforward approach than the use of two separate emitters (Fig. 9.4c). Herein, nonspecific environmental factors affecting the dye luminescence differently, concentration variations, and a different photostability are eliminated [98]. This design concept is seldom realized, particularly for small molecular sensors, because most emitters display only a single-luminescence band.

9.8 Surface-Enhanced Raman Scattering Diagnostics of Cancer

Currently, surface-enhanced Raman scattering (SERS) has been proved to be an ultrasensitive tool for noninvasively cancer cell detection and imaging in vitro and in vivo [105]. Successful realization of SERS experiments depends on interaction between adsorbed molecules and nanoparticles surface. Development of new synthesis methods of hybrid SERS-active nanostructures have the potential to improve the visualization, diagnostics of various diseases, therapy and drug delivery. SERS labels consisted of a hybrid material with Raman-active probe and a molecule capable of specific binding to the studied biological objects (antigen-antibody, ligand-receptor, enzyme-inhibitor), have a number of advantages over fluorescent labels, as they have greater sensitivity when detecting biological molecules.

For Raman tracking and imaging of drug release in tumors after nanodelivery, some of the most significant investigations have employed doxorubicin. For instance, Wang and co-workers synthesized folic acid (FA)-coated AgNPs in which FA acted as a specific targeting agent of the folate receptor expressed in the KB cancer cell and

a Raman-active molecule [106]. Besides, they conjugated the chemotherapeutic drug doxorubicin (DOX) to FA-AgNPs and investigated the efficiency of DOX delivery to the cancer cells using fluorescence lifetime imaging (FLIM). Thus, FA-AgNPs-DOX system showed excellent receptor-mediated cellular uptake. For the first time, Hossain et al. proposed biohybrid DOX-loaded gold nanoparticles with improved cell recognition by adding a penetrating trans-activator of transcription cysteine-modified (Tat-C) peptide in combination with the antibody-antigen targeted HER2 receptor [107]. They showed the possibility to characterize the intracellural DOX release inside SKBR-3 breast cancer cells by the releasing action of glutathione using in situ SERS monitoring.

Taking into account active targeting concerns, instead of doxorubicin, the other drugs have been suggested by other researches based on the principle of antibody-antigen recognition [108–110]. For Raman spectroscopy, one such drug is cetuximab, an epidermal growth factor receptor (EGFR) inhibitor used as anti-cancer agents. Molecular-plasmon hybrids using for SERS diagnostics of cancer have similar structures and integrate into single nanoplatform components having defined functional properties: (1) metallic nanoparticles as a core to perform photothermal therapy (PTT) and control a drug release; (2) PEG as biologically inert shell, protecting nanoparticles from immune system; (3) Raman-active molecule to enhance the intensity of SERS signal; and (4) anti-cancer agents for chemotherapy. For example, Conde et al. prepared gold nanoparticles coated by Raman-active molecule DTTC (3,3′-Diethylthiatricarbocyanine iodide) inside a polymer shell (HS-PEG) and after that covered with FDA approved cetuximab bonded via EDC (1-Ethyl-3-(3-dimethylaminopropyl) carbodiimide)/NHS (*N*-hydroxysuccinimide) coupling reaction, occurring between the carboxylated PEG and the terminal NH_2 group of the antibody. In such system they investigated in vivo ability of cetuximab attached at the surface of gold nanoprobes to target specific markers at the tumor surface [111]. Characteristic Raman spectra of drug–Raman NPs in HT-adenocarcinoma cells from colorectal cancer revealed a 4.5-fold higher signal of the characteristic Raman "fingerprint" of DTTC from the nanoparticles on the cell membrane than Raman-NPs only, showing a characteristic SERS peak at 518 cm^{-1}.

Also, hybrid nanostructures can be used in the construction of Raman scattering (SERS) nanotags for the photosensitizer's distribution in biopsied human cancerous and non-cancerous tissues. Using SERS technique, it may be possible in photosensitizer-functionalized GNPs to realize in real-time the following options, such as: (1) detection of the disease; (2) delivery the ROS agent directly to the tumor site; and (3) the quantitative dosage of photosensitizer required for efficient ROS conversion and damage [112, 113]. It has been reported that porphyrin derivatives are widely used as photosensitizers [114]. For example, Farhadi's group studied the palladium-doped photosensitizer pheophorbide A (Pd-pyrolipid) encapsulated at the surface of spherical AuNPs for monitoring the PDT by SERS [115]. Without using a Raman reporter, the researchers achieved the enhanced signal of the Pd-pyrolipid spectrum upon 638 nm wavelength laser excitation and generation of ROS species for PDT as well. SERS-active gold nanochains (AuNCs) consisted of AuNPs functionalized with a Raman reporter (2-naphthalenethiol) and a photosensitizer (Pheophorbide

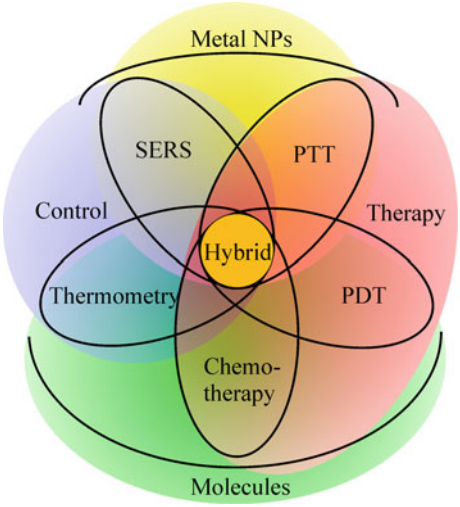

Fig. 9.5 The diagram of bio- and medicine hybrid nanostructures application

A) covalently attached to a polymeric chain of hyaluronic acid and hydrocaffeic acid (HA–HCA) has been synthesized [116]. Compared with the laser irradiated free photosensitizer, conjugated AuNCs exhibited the best absorption and SERS properties in the NIR spectral region as well as 99% cellular uptake and excellent phototoxicity, even at low photosensitizer concentrations.

Nowadays, newly synthesized analogues of heptamethine dyes such as 2-[2-[2-Chloro-3-[(1,3-dihydro-3,3-dimethyl-1-propyl-2*H*-indol-2-ylidene) ethylidene]-1-cyclohexen-1-yl]ethenyl]-3,3-dimethyl-1-propylindolium (IR780), 2-[2-[2-Chloro-3-[[1,3-dihydro-1,1-dimethyl-3-(4-sulfobutyl)-2*H*-benzo[e]indol-2-ylidene]-ethylidene]-1-cyclohexen-1-yl]-ethenyl]-1,1-dimethyl-3-(4-sulfobutyl)-1*H*-benzo[e]indolium (IR820), and 2-[2-[2-Chloro-3-[2-[1,3-dihydro-3,3-dimethyl-1-(5-carboxypentyl)-2*H*-indol-2-ylidene]-ethylidene]-1-cyclohexen-1-yl]-ethenyl]-3,3-dimethyl-1-(5-carboxypentyl)-3*H*-indolium bromide (MHI-148), which presents an opportunity in photothermal therapy (PTT), photodynamic therapy (PDT), and other combinatorial therapeutic methods, are promising materials for fabrication of hybrid nanoplatform due to its ability to generate heat upon laser irradiation, and generation of reactive oxygen species (ROS), such as singlet oxygen, acting as excellent photothermal and photodynamic agent simultaneously [117–119]. New theranostic nanoplatforms based on gold nanoparticles covered by different stabilizing agents and hydrophobic near infrared (NIR) dye, IR780 iodide, able to perform live cell imaging through surface-enhanced resonance Raman scattering (SERRS) microscopy [120, 121]. Subsequently, many researchers demonstrated the possibility to provide an accurate mapping of the cell using hybrid nanostructures due to strong, distinct intensity of SERS signal inside cells upon laser (785–808 nm) excitation.

All the examples considered can be summarized in the form of the diagram shown in the Fig. 9.5.

The diagram shows the correlation between composition, functional properties and application of hybrid nanostructures. The modern trends in hybrids design leads to the creation of universal structures in terms of controlled complex therapy. Thus, in the near future, the hybrids, which allow simultaneous implementation of PDT, PTT and chemotherapy, as well as local temperature control and tracking of the cancer cells destruction by SERS, will be constructed.

References

1. Y. Wang, F. Wang, Y. Shen et al., Tumor-specific disintegratable nanohybrids containing ultrasmall inorganic nanoparticles: from design and improved properties to cancer applications. Mater. Horizons **5**, 184–205 (2018)
2. H. Zhu, P. Cheng, P. Chen, K. Pu, Recent progress in the development of near-infrared organic photothermal and photodynamic nanotherapeutics. Biomater. Sci. **6**, 746–765 (2018)
3. S. Sreejith, T.T.M. Huong, P. Borah, Y. Zhao, Organic–inorganic nanohybrids for fluorescence, photoacoustic and Raman bioimaging. Sci. Bull. **60**, 665–678 (2015)
4. J. Zhou, P. Wang, C. Wang et al., Versatile core-shell nanoparticle@metal–organic framework nanohybrids: exploiting mussel-inspired polydopamine for tailored structural integration. ACS Nano **9**, 6951–6960 (2015). https://doi.org/10.1021/acsnano.5b01138
5. J. Song, X. Yang, O. Jacobson et al., Ultrasmall gold nanorod vesicles with enhanced tumor accumulation and fast excretion from the body for cancer therapy. Adv. Mater. **27**, 4910–4917 (2015)
6. J.-Y. Zeng, M.-K. Zhang, M.-Y. Peng et al., Porphyrinic metal-organic frameworks coated gold nanorods as a versatile nanoplatform for combined photodynamic/photothermal/chemotherapy of tumor. Adv. Funct. Mater. **28**, 1705451 (2018)
7. L. Jing, X. Liang, X. Li et al., Mn-porphyrin conjugated Au nanoshells encapsulating doxorubicin for potential magnetic resonance imaging and light triggered synergistic therapy of cancer. Theranostics **4**, 858–871 (2014)
8. D. Yang, J. Xu, G. Yang et al., Metal-organic frameworks join hands to create an anti-cancer nanoplatform based on 808 nm light driving up-conversion nanoparticles. Chem. Eng. J. **344**, 363–374 (2018)
9. Q. Mu, G. Jiang, L. Chen et al., Chemical basis of interactions between engineered nanoparticles and biological systems. Chem. Rev. **114**, 7740–7781 (2014)
10. R. Khandelia, A. Jaiswal, S.S. Ghosh, A. Chattopadhyay, Gold nanoparticle-protein agglomerates as versatile nanocarriers for drug delivery. Small **9**, 3494–3505 (2013)
11. Y. Ma, J. Huang, S. Song et al., Cancer-targeted nanotheranostics: recent advances and perspectives. Small **12**, 4936–4954 (2016)
12. C. Yi, S. Zhang, K.T. Webb, Z. Nie, Anisotropic self-assembly of hairy inorganic nanoparticles. Acc. Chem. Res. **50**, 12–21 (2017)
13. P.K. Jain, X. Huang, I.H. El-Sayed, M.A. El-Sayed, Noble metals on the nanoscale: optical and photothermal properties and some applications in imaging, sensing, biology, and medicine. Acc. Chem. Res. **41**, 1578–1586 (2008)
14. M. Kodiha, E. Hutter, S. Boridy et al., Gold nanoparticles induce nuclear damage in breast cancer cells, which is further amplified by hyperthermia. Cell. Mol. Life Sci. **71**, 4259–4273 (2014)
15. P. Mishra, S. Ray, S. Sinha et al., Facile bio-synthesis of gold nanoparticles by using extract of *Hibiscus sabdariffa* and evaluation of its cytotoxicity against U87 glioblastoma cells under hyperglycemic condition. Biochem. Eng. J. **105**, 264–272 (2016)
16. X. Kang, X. Guo, W. An et al., Photothermal therapeutic application of gold nanorods-porphyrin-trastuzumab complexes in HER2-positive breast cancer. Sci. Rep. **7**, 42069 (2017)

17. M.A. Mackey, M.R.K. Ali, L.A. Austin et al., The most effective gold nanorod size for plasmonic photothermal therapy: theory and in vitro experiments. J. Phys. Chem. B **118**, 1319–1326 (2014)
18. A. Ahmadi, S. Arami, Potential applications of nanoshells in biomedical sciences. J. Drug Target. **22**, 175–190 (2014)
19. M.E. Khosroshahi, Z. Hassannejad, M. Firouzi, A.R. Arshi, Nanoshell-mediated targeted photothermal therapy of HER2 human breast cancer cells using pulsed and continuous wave lasers: an in vitro study. Lasers Med. Sci. **30**, 1913–1922 (2015)
20. S.E. Skrabalak, J. Chen, L. Au et al., Gold nanocages for biomedical applications. Adv. Mater. **19**, 3177–3184 (2007)
21. C.M. Cobley, L. Au, J. Chen, Y. Xia, Targeting gold nanocages to cancer cells for photothermal destruction and drug delivery. Expert Opin. Drug Deliv. **7**, 577–587 (2010)
22. D. Jaque, L. Martínez Maestro, B. del Rosal et al., Nanoparticles for photothermal therapies. Nanoscale **6**, 9494–9530 (2014)
23. H. Shi, X. Ye, X. He et al., Au@Ag/Au nanoparticles assembled with activatable aptamer probes as smart "nano-doctors" for image-guided cancer thermotherapy. Nanoscale **6**, 8754 (2014)
24. J. Lin, Z. Huang, H. Wu et al., Inhibition of autophagy enhances the anticancer activity of silver nanoparticles. Autophagy **10**, 2006–2020 (2014)
25. R. Foldbjerg, E.S. Irving, Y. Hayashi et al., Global gene expression profiling of human lung epithelial cells after exposure to nanosilver. Toxicol. Sci. **130**, 145–157 (2012)
26. P. AshaRani, S. Sethu, H. Lim et al., Differential regulation of intracellular factors mediating cell cycle, DNA repair and inflammation following exposure to silver nanoparticles in human cells. Genome Integr **3**, 2 (2012)
27. D. Chen, S. Gao, W. Ge et al., One-step rapid synthesis of fluorescent platinum nanoclusters for cellular imaging and photothermal treatment. RSC Adv. **4**, 40141 (2014)
28. D. Chen, C. Zhao, J. Ye et al., In situ biosynthesis of fluorescent platinum nanoclusters: toward self-bioimaging-guided cancer theranostics. ACS Appl. Mater. Interfaces **7**, 18163–18169 (2015)
29. T.C. Johnstone, G.Y. Park, S.J. Lippard, Understanding and improving platinum anti-cancer drugs—phenanthriplatin. Anticancer Res. **34**, 471–476 (2014)
30. Z.S. Silva, S.K. Bussadori, K.P.S. Fernandes et al., Animal models for photodynamic therapy (PDT). Biosci. Rep. **35**, e00265–e00265 (2015)
31. G. Calixto, J. Bernegossi, L. de Freitas et al., Nanotechnology-based drug delivery systems for photodynamic therapy of cancer: a review. Molecules **21**, 342 (2016). https://doi.org/10.3390/molecules21030342
32. X. Li, S. Kolemen, J. Yoon, E.U. Akkaya, Activatable photosensitizers: agents for selective photodynamic therapy. Adv. Funct. Mater. **27**, 1604053 (2017)
33. X. Li, B.-D. Zheng, X.-H. Peng et al., Phthalocyanines as medicinal photosensitizers: developments in the last five years. Coord. Chem. Rev. (2017)
34. H. Eshghi, A. Sazgarnia, M. Rahimizadeh et al., Protoporphyrin IX–gold nanoparticle conjugates as an efficient photosensitizer in cervical cancer therapy. Photodiagnosis Photodyn. Ther. **10**, 304–312 (2013)
35. S.C. Hayden, L.A. Austin, R.D. Near et al., Plasmonic enhancement of photodynamic cancer therapy. J. Photochem. Photobiol. A Chem. **269**, 34–41 (2013)
36. K. Záruba, J. Králová, P. Řezanka et al., Modified porphyrin–brucine conjugated to gold nanoparticles and their application in photodynamic therapy. Org. Biomol. Chem. **8**, 3202 (2010)
37. O. Penon, T. Patiño, L. Barrios et al., A new porphyrin for the preparation of functionalized water-soluble gold nanoparticles with low intrinsic toxicity. ChemistryOpen **4**, 127–136 (2015)
38. Y. Guo, M. Kumar, P. Zhang, Nanoparticle-based photosensitizers under CW infrared excitation. Chem. Mater. **19**, 6071–6072 (2007)

39. K. Knop, A.-F. Mingotaud, N. El-Akra et al., Monomeric pheophorbide(a)-containing poly(ethyleneglycol-b-ε-caprolactone) micelles for photodynamic therapy. Photochem. Photobiol. Sci. **8**, 396 (2009)
40. Y. Hu, Y. Yang, H. Wang, H. Du, Synergistic integration of layer-by-layer assembly of photosensitizer and gold nanorings for enhanced photodynamic therapy in the near infrared. ACS Nano **9**, 8744–8754 (2015)
41. T.G. Shutava, S.S. Balkundi, P. Vangala et al., Layer-by-layer-coated gelatin nanoparticles as a vehicle for delivery of natural polyphenols. ACS Nano **3**, 1877–1885 (2009)
42. Z. Poon, D. Chang, X. Zhao, P.T. Hammond, Layer-by-layer nanoparticles with a pH-sheddable layer for in vivo targeting of tumor hypoxia. ACS Nano **5**, 4284–4292 (2011)
43. Z. Sheng, D. Hu, M. Zheng et al., Smart human serum albumin-indocyanine green nanoparticles generated by programmed assembly for dual-modal imaging-guided cancer synergistic phototherapy. ACS Nano **8**, 12310–12322 (2014)
44. S. Wang, P. Huang, L. Nie et al., Single continuous wave laser induced photodynamic/plasmonic photothermal therapy using photosensitizer-functionalized gold nanostars. Adv. Mater. **25**, 3055–3061 (2013)
45. A. Kumar, S. Kumar, W.-K. Rhim et al., Oxidative nanopeeling chemistry-based synthesis and photodynamic and photothermal therapeutic applications of plasmonic core-petal nanostructures. J. Am. Chem. Soc. **136**, 16317–16325 (2014)
46. M.E. Alea-Reyes, J. Soriano, I. Mora-Espí et al., Amphiphilic gemini pyridinium-mediated incorporation of Zn(II)meso-tetrakis(4-carboxyphenyl)porphyrin into water-soluble gold nanoparticles for photodynamic therapy. Colloids Surf. B Biointerfaces **158**, 602–609 (2017)
47. O. Penon, M.J. Marín, D.A. Russell, L. Pérez-García, Water soluble, multifunctional antibody-porphyrin gold nanoparticles for targeted photodynamic therapy. J. Colloid Interface Sci. **496**, 100–110 (2017)
48. H.S. Han, K.Y. Choi, H. Lee et al., Gold-nanoclustered hyaluronan nano-assemblies for photothermally maneuvered photodynamic tumor ablation. ACS Nano **10**, 10858–10868 (2016)
49. Y. Zheng, Y. Yuan, Y. Chai, R. Yuan, l-cysteine induced manganese porphyrin electrocatalytic amplification with 3D DNA-Au@Pt nanoparticles as nanocarriers for sensitive electrochemical aptasensor. Biosens. Bioelectron. **79**, 86–91 (2016)
50. K.S. Lokesh, A. Shambhulinga, N. Manjunatha et al., Porphyrin macrocycle-stabilized gold and silver nanoparticles and their application in catalysis of hydrogen peroxide. Dye Pigment **120**, 155–160 (2015)
51. J. Zeng, W. Yang, D. Shi et al., Porphyrin derivative conjugated with gold nanoparticles for dual-modality photodynamic and photothermal therapies in vitro. ACS Biomater. Sci. Eng. **4**, 963–972 (2018)
52. J. Lin, S. Wang, P. Huang et al., Photosensitizer-loaded gold vesicles with strong plasmonic coupling effect for imaging-guided photothermal/photodynamic therapy. ACS Nano **7**, 5320–5329 (2013)
53. Z. Wang, S. Sau, H.O. Alsaab, A,K, Iyer, CD44 directed nanomicellar payload delivery platform for selective anticancer effect and tumor specific imaging of triple negative breast cancer. Nanomed. Nanotechnol. Biol. Med. (2018)
54. X. Chen, W. Zhang, Diamond nanostructures for drug delivery, bioimaging, and biosensing. Chem. Soc. Rev. **46**, 734–760 (2017)
55. C. Ding, Z. Li, A review of drug release mechanisms from nanocarrier systems. Mater. Sci. Eng. C **76**, 1440–1453 (2017)
56. S. Chen, Q. Lei, W.-X. Qiu et al., Mitochondria-targeting "nanoheater" for enhanced photothermal/chemo-therapy. Biomaterials **117**, 92–104 (2017)
57. J. Nam, S. Son, L.J. Ochyl et al., Chemo-photothermal therapy combination elicits anti-tumor immunity against advanced metastatic cancer. Nat. Commun. **9**, 1074 (2018)
58. M.-Y. Lee, J.-A. Yang, H.S. Jung et al., Hyaluronic acid-gold nanoparticle/interferon α complex for targeted treatment of hepatitis C virus infection. ACS Nano **6**, 9522–9531 (2012)
59. Z. Wang, Z. Chen, Z. Liu et al., A multi-stimuli responsive gold nanocage–hyaluronic platform for targeted photothermal and chemotherapy. Biomaterials **35**, 9678–9688 (2014)

60. W. Chen, S. Zhang, Y. Yu et al., Structural-engineering rationales of gold nanoparticles for cancer theranostics. Adv. Mater. **28**, 8567–8585 (2016)
61. D. Luo, K.A. Carter, D. Miranda, J.F. Lovell, Chemophototherapy: an emerging treatment option for solid tumors. Adv. Sci. **4**, 1600106 (2017)
62. J. Park, J. Park, E.J. Ju et al., Multifunctional hollow gold nanoparticles designed for triple combination therapy and CT imaging. J. Control Release **207**, 77–85 (2015)
63. J.B. Weaver, Hot nanoparticles light up cancer. Nat. Nanotechnol. **5**, 630–631 (2010)
64. E.F.J. Ring, The historical development of temperature measurement in medicine. Infrared Phys. Technol. **49**, 297–301 (2007)
65. P.R.N. Childs, J.R. Greenwood, C.A. Long, Review of temperature measurement. Rev. Sci. Instrum. **71**, 2959–2978 (2000)
66. L. Michalski, K. Eckersdorf, J. Kucharski, J. McGhee, *Temperature Measurement*, 2nd ed. (Wiley, New York, 2001)
67. S. Maekawa, T. Tohyama, S.E. Barnes et al., *Physics of Transition Metal Oxides* (Springer, Berlin, 2004)
68. N.A.N. Mermin, *Solid State Physics* (Saunders College, Philadelphia, 1976)
69. M. Tabib-Azar, Optical temperature sensors, in *Integrated Optics, Microstructures, and Sensors* (Springer, Berlin, 1995), pp. 285–313
70. C.D.S. Brites, P.P. Lima, N.J.O. Silva et al., Thermometry at the nanoscale. Nanoscale **4**, 4799 (2012)
71. G.F. Imbusch, B. Henderson, *Optical Spectroscopy of Inorganic Solids* (Oxford Science Publications, London, 2006)
72. D. Jaque, F. Vetrone, Luminescence nanothermometry. Nanoscale **4**, 4301 (2012)
73. M. Engeser, L. Fabbrizzi, M. Licchelli, D. Sacchi, A fluorescent molecular thermometer based on the nickel(II) high-spin/low-spin interconversion. Chem. Commun. 1191–1192 (1999)
74. R. Samy, T. Glawdel, C.L. Ren, Method for microfluidic whole-chip temperature measurement using thin-film poly(dimethylsiloxane)/rhodamine B. Anal. Chem. **80**, 369–375 (2008)
75. V.M. Chauhan, R.H. Hopper, S.Z. Ali et al., Thermo-optical characterization of fluorescent rhodamine B based temperature-sensitive nanosensors using a CMOS MEMS micro-hotplate. Sens. Actuators B Chem. **192**, 126–133 (2014)
76. D. Ross, M. Gaitan, L.E. Locascio, Temperature measurement in microfluidic systems using a temperature-dependent fluorescent dye. Anal. Chem. **73**, 4117–4123 (2001)
77. F.-L. Mi, Synthesis and characterization of a novel chitosan–gelatin bioconjugate with fluorescence emission. Biomacromol **6**, 975–987 (2005)
78. K. Miyata, Y. Konno, T. Nakanishi et al., Chameleon luminophore for sensing temperatures: control of metal-to-metal and energy back transfer in lanthanide coordination polymers. Angew Chem. Int. Ed. **52**, 6413–6416 (2013)
79. J.M. Lupton, A molecular thermometer based on long-lived emission from platinum octaethyl porphyrin. Appl. Phys. Lett. **81**, 2478–2480 (2002)
80. D. Cauzzi, R. Pattacini, M. Delferro et al., Temperature-dependent fluorescence of Cu5 metal clusters: a molecular thermometer. Angew Chem. Int. Ed. **51**, 9662–9665 (2012)
81. S. Otto, N. Scholz, T. Behnke et al., Thermo-chromium: a contactless optical molecular thermometer. Chem. A Eur. J. **23**, 12131–12135 (2017)
82. J. Feng, K. Tian, D. Hu et al., A Triarylboron-based fluorescent thermometer: sensitive over a wide temperature range. Angew Chem. Int Ed. **50**, 8072–8076 (2011)
83. B. Huitorel, Q. Benito, A. Fargues et al., Mechanochromic luminescence and liquid crystallinity of molecular copper clusters. Chem. Mater. **28**, 8190–8200 (2016)
84. F. Parmeggiani, A. Sacchetti, Preparation and luminescence thermochromism of tetranuclear copper(I)–pyridine–iodide clusters. J. Chem. Educ. **89**, 946–949 (2012)
85. A. Yadav, A.K. Srivastava, A. Balamurugan, R. Boomishankar, A cationic copper(I) iodide cluster MOF exhibiting unusual ligand assisted thermochromism. Dalt. Trans. **43**, 8166–8169 (2014)
86. G. Baffou, M.P. Kreuzer, F. Kulzer, R. Quidant, Temperature mapping near plasmonic nanostructures using fluorescence polarization anisotropy. Opt. Express **17**, 3291 (2009)

87. J.S. Donner, S.A. Thompson, M.P. Kreuzer et al., Mapping intracellular temperature using green fluorescent protein. Nano Lett. **12**, 2107–2111 (2012)
88. I.E. Kolesnikov, A.A. Kalinichev, M.A. Kurochkin et al., YVO4:Nd^{3+} nanophosphors as NIR-to-NIR thermal sensors in wide temperature range. Sci. Rep. **7**, 18002 (2017)
89. I.E. Kolesnikov, E.V. Golyeva, A.A. Kalinichev et al., Nd^{3+} single doped YVO 4 nanoparticles for sub-tissue heating and thermal sensing in the second biological window. Sens. Actuators B Chem. **243**, 338–345 (2017)
90. A. Benayas, E. Escuder, D. Jaque, High-resolution confocal fluorescence thermal imaging of tightly pumped microchip Nd:YAG laser ceramics. Appl. Phys. B **107**, 697–701 (2012)
91. A.A. Kaminskii, Laser crystals and ceramics: recent advances. Laser Photon. Rev. **1**, 93–177 (2007)
92. D. Moreau, C. Lefort, R. Burke et al., Rhodamine B as an optical thermometer in cells focally exposed to infrared laser light or nanosecond pulsed electric fields. Biomed. Opt. Express **6**, 4105 (2015)
93. T. Karstens, K. Kobs, Rhodamine B and rhodamine 101 as reference substances for fluorescence quantum yield measurements. J. Phys. Chem. **84**, 1871–1872 (1980)
94. D.A. Mendels, E.M. Graham, S. Magennis et al., Quantitative comparison of thermal and solutal transport in a T-mixer by FLIM and CFD. Microfluid. Nanofluid. **5**, 603–617 (2008)
95. L.-N. Sun, J. Yu, H. Peng et al., Temperature-sensitive luminescent nanoparticles and films based on a terbium (III) complex probe. J. Phys. Chem. C **114**, 12642–12648 (2010)
96. C.D.S. Brites, P.P. Lima, N.J.O. Silva et al., A luminescent molecular thermometer for long-term absolute temperature measurements at the nanoscale. Adv. Mater. **22**, 4499–4504 (2010)
97. J.-H. Wang, M. Li, J. Zheng et al., A dual-emitting Cu 6-Cu 2-Cu 6 cluster as a self-calibrated, wide-range luminescent molecular thermometer. Chem. Commun. **50**, 9115–9118 (2014)
98. X. Wang, O.S. Wolfbeis, R.J. Meier, Luminescent probes and sensors for temperature. Chem. Soc. Rev. **42**, 7834 (2013)
99. H. Zhou, M. Sharma, O. Berezin et al., Nanothermometry: from microscopy to thermal treatments. ChemPhysChem **17**, 27–36 (2016)
100. M. Schäferling, The art of fluorescence imaging with chemical sensors. Angew Chem. Int. Ed. **51**, 3532–3554 (2012)
101. C. Nellaker, U. Wallgren, H. Karlsson, Molecular beacon-based temperature control and automated analyses for improved resolution of melting temperature analysis using SYBR I green chemistry. Clin. Chem. **53**, 98–103 (2006)
102. G. Ke, C. Wang, Y. Ge et al., L-DNA molecular beacon: a safe, stable, and accurate intracellular nano-thermometer for temperature sensing in living cells. J. Am. Chem. Soc. **134**, 18908–18911 (2012)
103. S. Ebrahimi, Y. Akhlaghi, M. Kompany-Zareh, Å. Rinnan, Nucleic acid based fluorescent nanothermometers. ACS Nano **8**, 10372–10382 (2014)
104. Z. Fidan, A. Wende, U. Resch-Genger, Visible and red emissive molecular beacons for optical temperature measurements and quality control in diagnostic assays utilizing temperature-dependent amplification reactions. Anal. Bioanal. Chem. **409**, 1519–1529 (2017)
105. E. Darrigues, V. Dantuluri, Z.A. Nima et al., Raman spectroscopy using plasmonic and carbon-based nanoparticles for cancer detection, diagnosis, and treatment guidance. Part 2: treatment. Drug Metab. Rev. **49**, 253–283 (2017)
106. Y. Wang, B.B. Newell, J. Irudayaraj, Folic acid protected silver nanocarriers for targeted drug delivery. J. Biomed. Nanotechnol. **8**, 751–759 (2012)
107. M.K. Hossain, H.-Y. Cho, K.-J. Kim, J.-W. Choi, In situ monitoring of doxorubicin release from biohybrid nanoparticles modified with antibody and cell-penetrating peptides in breast cancer cells using surface-enhanced Raman spectroscopy. Biosens. Bioelectron. **71**, 300–305 (2015)
108. C. Peters, S. Brown, Antibody-drug conjugates as novel anti-cancer chemotherapeutics. Biosci. Rep. **35**, e00225–e00225 (2015)
109. S. Nussbaumer, P. Bonnabry, J.-L. Veuthey, S. Fleury-Souverain, Analysis of anticancer drugs: a review. Talanta **85**, 2265–2289 (2011)

110. H.-W. Kao, Y.-Y. Lin, C.-C. Chen et al., Biological characterization of cetuximab-conjugated gold nanoparticles in a tumor animal model. Nanotechnology **25**, 295102 (2014)
111. J. Conde, C. Bao, D. Cui et al., Antibody–drug gold nanoantennas with Raman spectroscopic fingerprints for in vivo tumour theranostics. J. Control Release **183**, 87–93 (2014)
112. J. Feng, L. Chen, Y. Xia et al., Bioconjugation of gold nanobipyramids for SERS detection and targeted photothermal therapy in breast cancer. ACS Biomater. Sci. Eng. **3**, 608–618 (2017)
113. J. Song, L. Pu, J. Zhou et al., Biodegradable theranostic plasmonic vesicles of amphiphilic gold nanorods. ACS Nano **7**, 9947–9960 (2013)
114. A.M. Fales, H. Yuan, T. Vo-Dinh, Cell-penetrating peptide enhanced intracellular raman imaging and photodynamic therapy. Mol. Pharm. **10**, 2291–2298 (2013)
115. A. Farhadi, Á. Roxin, B.C. Wilson, G. Zheng, Nano-enabled SERS reporting photosensitizers. Theranostics **5**, 469–476 (2015)
116. L. Zhao, T.-H. Kim, H.-W. Kim et al., Surface-enhanced Raman scattering (SERS)-active gold nanochains for multiplex detection and photodynamic therapy of cancer. Acta Biomater. **20**, 155–164 (2015)
117. C. Pais-Silva, D. de Melo-Diogo, I.J. Correia, IR780-loaded TPGS-TOS micelles for breast cancer photodynamic therapy. Eur. J. Pharm. Biopharm. **113**, 108–117 (2017)
118. S. Harmsen, M.A. Wall, R. Huang, M.F. Kircher, Cancer imaging using surface-enhanced resonance Raman scattering nanoparticles. Nat. Protoc. **12**, 1400–1414 (2017)
119. A. Yuan, J. Wu, X. Tang et al., Application of near-infrared dyes for tumor imaging, photothermal, and photodynamic therapies. J. Pharm. Sci. **102**, 6–28 (2013)
120. C.G. Alves, R. Lima-Sousa, D. de Melo-Diogo et al., IR780 based nanomaterials for cancer imaging and photothermal, photodynamic and combinatorial therapies. Int. J. Pharm. **542**, 164–175 (2018)
121. T. Nagy-Simon, M. Potara, A.-M. Craciun et al., IR780-dye loaded gold nanoparticles as new near infrared activatable nanotheranostic agents for simultaneous photodynamic and photothermal therapy and intracellular tracking by surface enhanced resonant Raman scattering imaging. J. Colloid Interface Sci. **517**, 239–250 (2018)